Applied Physics Letters

Current-driven magnetic skyrmion diodes controlled by voltage gates in synthetic antiferromagnets

Cite as: Appl. Phys. Lett. **122**, 152404 (2023); https://doi.org/10.1063/5.0142460
Submitted: 13 January 2023 • Accepted: 31 March 2023 • Published Online: 11 April 2023

Min Xu, Zhiyu Zhang, Jinyu Zhang, et al.

AIP Publishing

Applied Physics Letters ARTICLE scitation.org/journal/apl

Current-driven magnetic skyrmion diodes controlled by voltage gates in synthetic antiferromagnets

Cite as: Appl. Phys. Lett. **122**, 152404 (2023); doi: 10.1063/5.0142460
Submitted: 13 January 2023 · Accepted: 31 March 2023 ·
Published Online: 11 April 2023

Min Xu,[a] Zhiyu Zhang,[a] Jinyu Zhang, Guiqian Jiang, Yuliang Chen, Wenlong Chen, and Changjing Hu

AFFILIATIONS

Key Laboratory for Anisotropy and Texture of Materials (MOE), School of Materials Science and Engineering, Northeastern University, Shenyang 110819, China

[a]Authors to whom correspondence should be addressed: xum@smm.neu.edu.cn and zhiyufine@foxmail.com

ABSTRACT

Magnetic skyrmions, as promising candidates in various spintronic devices, have been widely studied owing to their particle-like properties, nanoscale size, and low driving current density. Here, we numerically and theoretically investigate the dynamics of current-driven skyrmion passing through a voltage gate in a synthetic antiferromagnetic racetrack. It is found that the critical current required for skyrmion to pass through the voltage gate positively is much less than that for skyrmion to pass through the gate negatively. Furthermore, we systematically study the linear dependence of the minimum velocity of skyrmion on the driving current density and perpendicular magnetic anisotropy (PMA) gradient, and the calculation results are quite consistent with the simulation results. Finally, we find that the variation of the PMA energy with the position of skyrmion can help us to compare the magnitude of resistance force when the skyrmion passes through different voltage gates. Our results can be beneficial for the design and development of skyrmion diodes.

Magnetic skyrmions are topologically protected spin textures with particle-like properties,[1–5] which were first experimentally observed in 2009.[6] Since then, skyrmions have been intensively investigated in the fields of magnetism and spintronics owing to their topological stability, nanoscale size, and low driving current density.[7–11] Moreover, their potential applications are extremely attractive, for example, as information carriers in racetrack memories,[12–14] spin-torque nano-oscillators,[15–17] and diodes.[18–20] In recent years, some experiments have confirmed that skyrmions can be created and driven by a spin-polarized current at room temperature, which is of significance for realizing skyrmion-based spintronic devices.[21–23]

However, no matter what method is applied to drive skyrmions, such as spin currents,[24–26] spin waves,[27–29] and perpendicular magnetic anisotropy (PMA) gradients,[30–32] these skyrmions always acquire a transverse velocity component and, therefore, lead to the annihilation at the edge of narrow tracks. This effect of skyrmions originates from their non-zero topological charge, which is similar to the Hall effect of charged particles, and therefore, it is called the skyrmion Hall effect (SkHE).[25,33,34] In order to avoid SkHE in certain applications of skyrmions, several methods have been proposed, such as creating a skyrmionium with zero topological charge in ferromagnetic (FM) materials,[27,35,36] driving a skyrmion by spin current in a synthetic antiferromagnetic (SAF) bilayer system,[21,37,38] and generating a monolayer antiferromagnetic (AFM) skyrmion.[16,39,40] One of the most promising approaches is generating and driving skyrmions in a synthetic antiferromagnetic (SAF) racetrack, which consists of two ferromagnetic layers antiferromagnetically coupled via a non-magnetic spacer layer, by the Ruderman–Kittel–Kasuya–Yoshida (RKKY) interlayer coupling.[41] In this system, the two antiferromagnetically coupled skyrmions in the top and bottom layers have opposite topological charges, resulting in a zero total topological charge.

In addition, the discovery and development of voltage-controlled magnetic anisotropy (VCMA) have had a marked impact on the application of skyrmions.[42,43] VCMA is a technique for changing the magnetic anisotropy of materials by applying an electric field, which has been used in various materials, such as Co/Ni,[44] MgO/FePt/Pt,[45] and Pt/Co.[46] In 2009, Maruyama *et al.* reported that the PMA can be changed by about 40% by applying a small electric field of less than 100 mV/nm in a Fe/MgO junction.[47] In many reports, VCMA is not only used to raise the PMA at the edge of racetracks to prevent the

annihilation of skyrmions but also used to generate a PMA gradient to drive skyrmions with low energy consumption, which facilitates the application of skyrmions on various electronic devices.[48–50]

In this paper, we numerically study the dynamics of skyrmions driven by a spin current in an SAF racetrack with VCMA. Our results show that the critical current required for skyrmion to positively pass through a voltage gate where the PMA constant increases gradually is much less than that for skyrmion to negatively pass through the voltage gate where the PMA constant decreases gradually, and skyrmion diodes can be designed based on this property. Furthermore, we numerically and theoretically investigate the minimum velocity of skyrmion as a function of the driving current density and the PMA gradient induced by the voltage gate when the skyrmion passing through the gate positively and negatively. Finally, we study the variation of PMA energy of skyrmion with its position, which makes it more convenient to compare the magnitude of resistance when the skyrmion passes through different voltage gates. This work is beneficial for designing voltage-controlled skyrmion diodes.

We perform micromagnetic simulations by using the Ubermag package,[51] which numerically solves the Landau–Lifshitz–Gilbert (LLG) equation with spin transfer torques (STT) as follows:

$$\frac{d\boldsymbol{m}}{dt} = -\gamma_0 \boldsymbol{m} \times \boldsymbol{H}_{eff} + \alpha\left(\boldsymbol{m} \times \frac{d\boldsymbol{m}}{dt}\right) + u(\boldsymbol{m} \times \boldsymbol{m_p} \times \boldsymbol{m}) - \beta u(\boldsymbol{m} \times \boldsymbol{m_p}), \quad (1)$$

where $\boldsymbol{m} = \boldsymbol{M}/M_s$, M_s is the saturation magnetization, γ_0 is the gyromagnetic ratio with an absolute value, α is the Gilbert damping coefficient, $\boldsymbol{m_p}$ is the unit spin polarization direction, $\boldsymbol{H_{eff}}$ is the effective field including the Heisenberg exchange, the Dzyaloshinskii–Moriya interaction (DMI), the PMA, the demagnetization, and the RKKY coupling. $u = |\frac{\gamma_0 \hbar}{\mu_0 e}|\frac{JP}{2M_s}$ is the STT coefficient, β is the strength of non-adiabatic STT torque, $\hbar$ is the reduced Plank constant, J is the applied current density, e is the electron charge, μ_0 is the vacuum permeability, and P is the spin polarizability. In our Pt/Ru/Co multilayer system, the magnetic parameters are as follows: $M_s = 580\,\mathrm{kA/m}$, the PMA constant $K_u = 0.8\,\mathrm{MJ/m^3}$, the DMI constant $D = 3\,\mathrm{mJ/m^2}$, the Heisenberg exchange constant $A = 15\,\mathrm{pJ/m}$, $\alpha = 0.1$, and the bilinear interfacial exchange coefficient $\sigma = -2\,\mathrm{mJ/m^2}$.

This simulation model is an SAF racetrack with two FM layers of $400 \times 100 \times 1\,\mathrm{nm^3}$ and a non-magnetic spacer layer, as shown in Fig. 1. The discretization size is set to $2 \times 2 \times 1\,\mathrm{nm^3}$. A wedge-shaped voltage gate, consisting of an electrode and an isolation layer, is set on the FM layer, and the insulation layer thickness ($t_{insulator}$) increases along the $+x$ direction. The gate can effectively modulate the anisotropy energy density, which is given by $\Delta PMA = |aE|$, where a and E are the coefficient of electric field-controlled magnetic anisotropy and the applied electric field, respectively, and $a \propto t_{insulator}$. Therefore, the gradient of $t_{insulator}$ causes the gradient of PMA in the gate.[52] In the simulation, the PMA constant $K_v(x)$ in the gate increases linearly along the $+x$ direction, denoted as[32] $K_v(x) = K_u + (x - x_0)\Delta K/L$ for $x \in [x_0, x_0 + L]$ and $\Delta K = K_{uv} - K_u$. K_{uv} is the maximum PMA constant in the gate, L is the length of the gate, and x_0 is the position of the gate. The anisotropy curve along the racetrack is displayed in Fig. S1 in the supplementary material.

In Fig. 2(a), when $J_{spin} = 10\,\mathrm{MA/cm^2}$, the skyrmion reaches the minimum velocity near the right end of the voltage gate and returns to its initial speed after leaving the voltage gate completely. We have marked the initial position, the position at the minimum speed ($P_{V_{min}}$), and the end position when the skyrmion passing through the voltage gate in Fig. 2(c). However, as J_{spin} drops to $3\,\mathrm{MA/cm^2}$, the velocity of the skyrmion near the left end of the voltage gate decreases to 0, indicated in Fig. 2(e). As revealed in Fig. 2(b), when the skyrmion is driven by reverse currents, it moves from right to left, and its velocity drops sharply near the right side of the voltage gate. Here, we specify that the motion direction of skyrmion from left to right is positive, while the direction from right to left is negative. It is found that the skyrmion can pass through the voltage gate at $J_{spin} = -20\,\mathrm{MA/cm^2}$, but is pinned at $J_{spin} = -10\,\mathrm{MA/cm^2}$, exhibited in Figs. 2(d) and 2(f). The reasons for the variation of skyrmion velocity at different stages

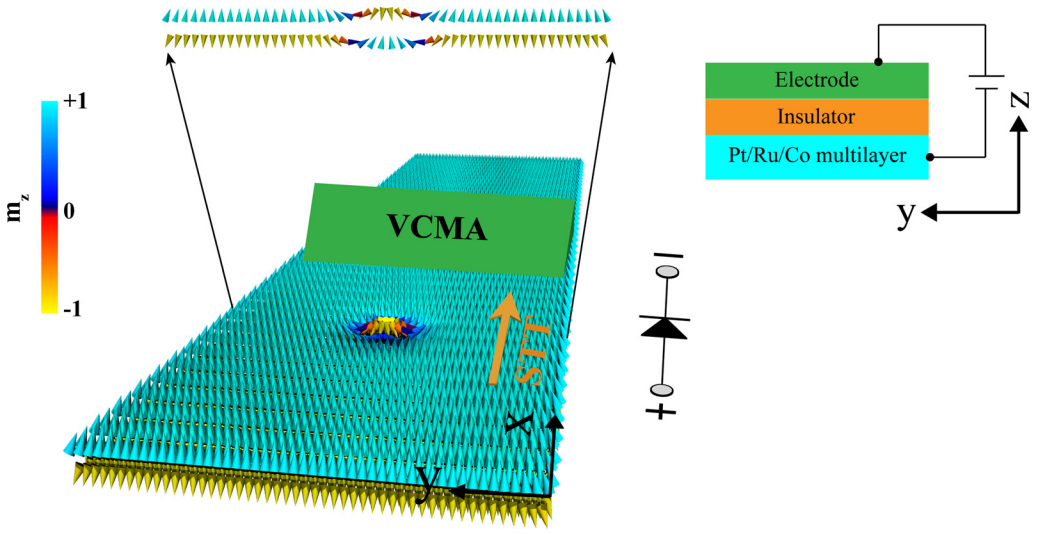

FIG. 1. Schematic illustration of a skyrmion diode controlled by the voltage gate. The two arrows point to the section of the model where a skyrmion is located.

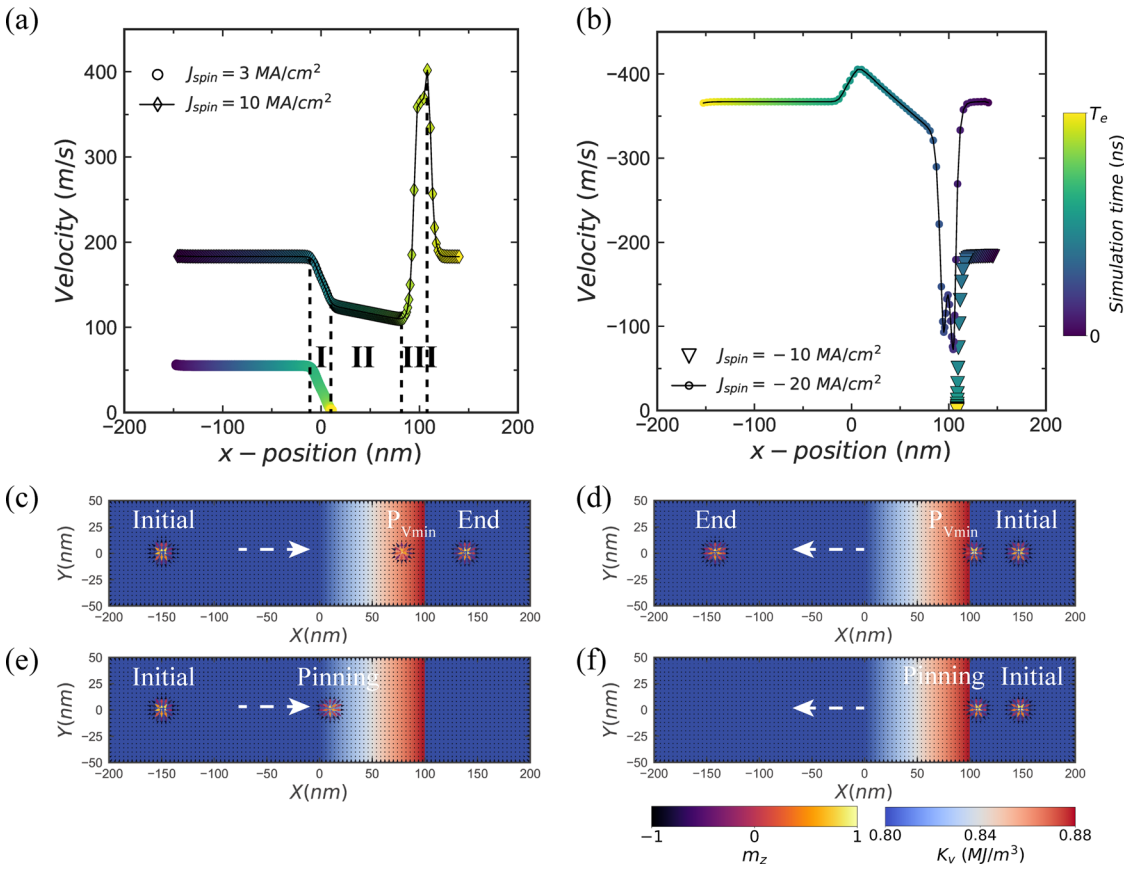

FIG. 2. The skyrmion driven by different currents when passing through a voltage gate with $L = 100$ nm and $\Delta K = 0.08\,\mathrm{MJ/m^3}$. (a) and (b) The velocity as a function of the position of the skyrmion under different directions and magnitudes of current (J_{spin}). T_e denotes the simulation end time, which varies with J_{spin}. (c) and (e) The positive motions of the skyrmion at $J_{spin} = 10\,\mathrm{MA/cm^2}$ and $J_{spin} = 3\,\mathrm{MA/cm^2}$, respectively. (d) and (f) The negative motions of the skyrmion at $J_{spin} = -20\,\mathrm{MA/cm^2}$ and $J_{spin} = -10\,\mathrm{MA/cm^2}$, respectively.

when skyrmion passing through different voltage gates are shown in the Figs. S2–S4 in the supplementary material.

The above-mentioned results demonstrate that the current required for skyrmion to pass the voltage gate positively is much smaller than that required for skyrmion to pass the gate negatively, which is the principle of the voltage-controlled skyrmion diode. Moreover, the minimum velocity of skyrmion ($V_{\min}$) can be used as an indicator of whether it can pass the voltage gate. $|V_{\min}| > 0$ denotes passing, while $|V_{\min}| = 0$ denotes being pinned.

In Fig. 3(a), it is found that $V_{\min}$ increases with increasing J_{spin} under certain L and ΔK, i.e., $V_{\min} \propto J_{spin}$. In addition, the critical current J_0, defined as the minimum current that the skyrmion can pass through the voltage gate, increases remarkably with decreasing L for $J_{spin} > 0$. However, the effect of L on J_0 is not noticeable for $J_{spin} < 0$. For example, as L decreases from 100 to 20 nm, J_0 goes from 3 to 11 $\mathrm{MA/cm^2}$ for $J_{spin} > 0$, while J_0 decreases from −16 to −13 $\mathrm{MA/cm^2}$ for $J_{spin} < 0$.

As shown in Fig. 3(b), the absolute value of J_0 for the positive motion of the skyrmion is much smaller than that for the negative motion at the same ΔK. For instance, when $\Delta K = 0.04\,\mathrm{MJ/m^3}$, $J_0 = 2\,\mathrm{MA/cm^2}$ for the positive motion ($J_{spin} > 0$), while $J_0 = -8\,\mathrm{MA/cm^2}$ for the negative motion ($J_{spin} < 0$). In addition, J_0 increases with the increase in ΔK for both $J_{spin} > 0$ and $J_{spin} < 0$, while with the increase in L, J_0 decreases for $J_{spin} > 0$ and increases for $J_{spin} < 0$. The effect of ΔK on J_0 for $J_{spin} > 0$ is greater than that for $J_{spin} < 0$, which is different from the effect of L on J_0. From the results of simulation, the J_{spin}–$V_{\min}$ characteristics of the skyrmion diode are similar to the volt–ampere characteristics of the electronic diode.

The simulation results reveal that $V_{\min}$ is linearly related to J_{spin}. In order to explore this dependence numerically, we use the Thiele equation to describe the motion of current-driven skyrmion in a two-layer system with a voltage gate,[36,37]

$$\boldsymbol{G}^{\boldsymbol{i}} \times \boldsymbol{v}^{\boldsymbol{i}} - \alpha \boldsymbol{D}^{\boldsymbol{i}} \cdot \boldsymbol{v}^{\boldsymbol{i}} + \boldsymbol{B}^{\boldsymbol{i}} \cdot \boldsymbol{J}^{\boldsymbol{i}} - \boldsymbol{F}^{\boldsymbol{i}}_{\boldsymbol{VGF}} = 0, \tag{2}$$

where i = top, bottom, the gyromagnetic coupling vector $\boldsymbol{G} = (0, 0, Q)$ with $Q = -\int d^2\boldsymbol{r} \cdot \boldsymbol{m} \cdot (\partial_x \boldsymbol{m} \times \partial_y \boldsymbol{m})/4\pi$, $\boldsymbol{v}$ is the velocity of skyrmion, $\boldsymbol{D}$ is the dissipation tensor, and $\boldsymbol{B}$ is the tensor linked to the STT. The components are calculated by $D_{\mu\nu} = \int d^2\boldsymbol{r} \cdot (\partial_\mu \boldsymbol{m} \cdot \partial_\nu \boldsymbol{m})/4$ and $B_{\mu\nu} = \frac{\mu}{aj} \int d^2\boldsymbol{r} \cdot (\partial_\mu \boldsymbol{m} \times \boldsymbol{m})_\nu / 4\pi$, where a is the thickness of each FM layer and μ and ν run over x and y. Both tensors $\boldsymbol{B}$ and $\boldsymbol{D}$ are related to the magnetization distribution of the skyrmion. $\boldsymbol{F}_{\boldsymbol{VGF}}$ is the force acting on the skyrmion, which arises from the inhomogeneous distribution of PMA energy induced by the voltage gate, expressed as[30,31,50]

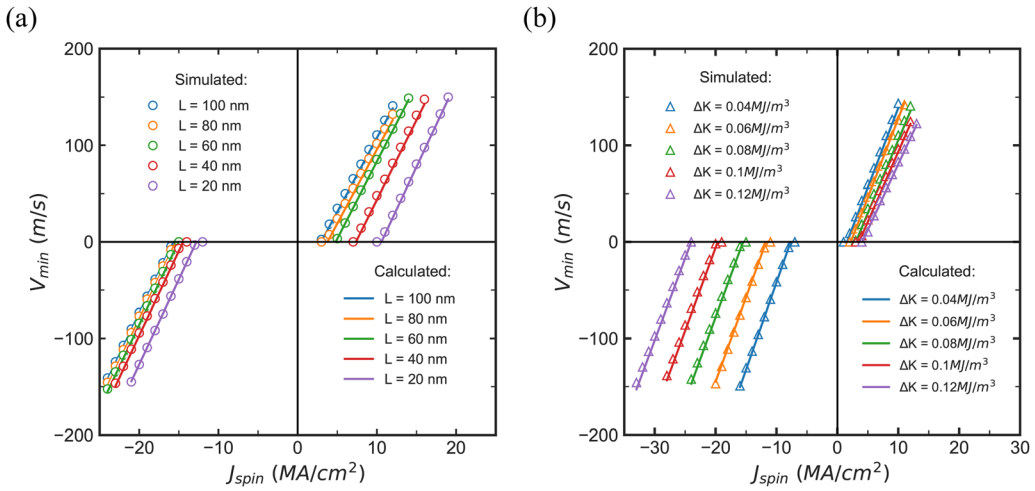

FIG. 3. (a) $V_{\min}$ as a function of J_{spin} at different L. (b) $V_{\min}$ as a function of J_{spin} at different ΔK.

$$\boldsymbol{F}_{VGF} = \frac{\gamma_0}{4\pi\mu_0 M_s}\frac{-\partial E_{K_u}}{\partial x}, \tag{3}$$

$$E_{K_u} = -K_v \int \left(1 - m_z^2\right) dxdy, \tag{4}$$

where E_{K_u} is the PMA energy of the skyrmion and the direction of $\boldsymbol{F}_{VGF}$ is toward the lower K_v region from the higher K_v region. When the skyrmion moves steadily in the voltage gate, $\frac{\partial E_{K_u}}{\partial x} = \frac{\partial E_{K_u}}{\partial K_v}\frac{\partial K_v}{\partial x}$.

For the skyrmion in each FM layer, $\boldsymbol{G}^{top} = -\boldsymbol{G}^{bottom}$, $\boldsymbol{D}^{top} = \boldsymbol{D}^{bottom}$, $\boldsymbol{v}^{top} = \boldsymbol{v}^{bottom}$. Meanwhile, $\boldsymbol{B}^{top} = 0$ and $\boldsymbol{B}^{bottom} = \boldsymbol{B}$ in as much as the spin current is applied to the bottom layer. The voltage gate is set at the same x coordinate of both FM layers, which means $\boldsymbol{F}_{VGF}^{top} = \boldsymbol{F}_{VGF}^{bottom}$. Therefore, Eq. (2) can be simplified as

$$-2\alpha D_{xx} v_x + B_{xy} J - 2F_{VGF} = 0. \tag{5}$$

From Eq. (5), the velocity of skyrmion in the voltage gate during the positive motion can be described as

$$v_x = \frac{1}{2\alpha D_{xx}}\frac{I_{xy}}{a}\,u(J) - \frac{C_z}{\alpha D_{xx}}\frac{\gamma_0}{\mu_0 M_s}\frac{\Delta K}{L}, \quad J > 0, \tag{6}$$

where $I_{xy} = -\int d^2\boldsymbol{r}\cdot(\partial_x \boldsymbol{m}\times\boldsymbol{m})_y/4\pi$, $C_z = \int d^2 r\left(1 - m_z^2\right)/4\pi$, and $u(J)$ denotes u as a function of J.

The first term on the right of Eq. (6) is the velocity of skyrmion outside the voltage gate, and the second term represents the hindrance of PMA gradient to the velocity of skyrmion in the voltage gate. It is notable that the process of the skyrmion passing through the voltage gate consists of three stages: entering the gate (I), moving in the gate (II), and leaving the gate (III), as illustrated in Fig. 2(a). Equation (6) is valid only for the stage II, but v_x drops slightly as the skyrmion enters the higher PMA region, revealed in Fig. S5(a) in the supplementary material. This can be explained by the fact that the skyrmion size decreases progressively when the skyrmion moves from the lower PMA region to the higher PMA region, resulting in small changes of D_{xx}, I_{xy}, and C_z, which may lead to the decrease in v_x according to Eq. (6).

In order to calculate $V_{\min}$ by Eq. (6), we first calculate the values of D_{xx}, I_{xy}, and C_z when the skyrmion has the minimum simulation velocity. From Eq. (6), the minimum velocity of skyrmion during the positive motion can be denoted as

$$V_{\min} = kJ + b, \quad J > 0, \tag{7}$$

where $k = \frac{I_{xy}}{2\alpha D_{xx}}\frac{u(J)}{aJ}$, $b = \frac{-C_z}{\alpha D_{xx}}\frac{\gamma_0}{\mu_0 M_s}\frac{\Delta K}{L}$, and the relevant parameters are given in Tables SI and SIII in the supplementary material. It is found that the calculated values fit well with the simulated values, see Fig. 3. However, when L is shorter than skyrmion diameter d, the skyrmion cannot move stably in the voltage gate, resulting in the calculated $V_{\min}$ less than the corresponding simulated values. To make the calculated value better fit the simulated value when $L < d$, b can be modified to $b' = \frac{1}{\alpha D_{xx}}\frac{\gamma_0}{4\pi\mu_0 M_s}\frac{\partial E_{K_u}}{\partial x}$ based on Eqs. (3) and (5).

Considering that we cannot accurately obtain the continuous variation of E_{K_u} in the x direction, i.e., $\frac{\partial E_{K_u}}{\partial x}$, we use the discretization method to approximate it, which means measuring the change in PMA energy at adjacent positions of the skyrmion. Since the time step in the simulation is extremely small, $\frac{\partial E_{K_u}}{\partial x} \approx \frac{\delta E_{K_u}}{\delta x}$, in which $\frac{\delta E_{K_u}}{\delta x} = \frac{E_{K_{u_{i+1}}} - E_{K_{u_i}}}{x_{i+1} - x_i}$.

In Fig. 4(a), we measure the position (x_i) of skyrmion at the minimum velocity, the PMA energy ($E_{K_{u_i}}$) of skyrmion at this position, and the previous position (x_{i-1}) and PMA energy ($E_{K_{u_{i-1}}}$) to calculate $\frac{\delta E_{K_u}}{\delta x}$, which represents the average force induced by the PMA gradient on the skyrmion in the extremely short distance ($x_i - x_{i-1}$). The result shows that b' and $V_{\min}$ calculated by this method are very close to the simulated values, as indicated in Fig. 3(a) and Table SI in the supplementary material.

When the skyrmion enters the voltage gate negatively, the PMA energy and velocity of skyrmion vary considerably in a short distance, which leads to a large variation of $\frac{\delta E_{K_u}}{\delta x}$ near the position where skyrmion has the minimum velocity as revealed in Fig. S5(b) in the supplementary material. In this case, it will cause a large error if $\frac{\partial E_{K_u}}{\partial x}$ is estimated by $\frac{\delta E_{K_u}}{\delta x}$. However, in Fig. 4(b), it is found that the skyrmion velocity decreases almost linearly when the skyrmion moves from the position (x_1) where the velocity begins to decline to the position (x_2)

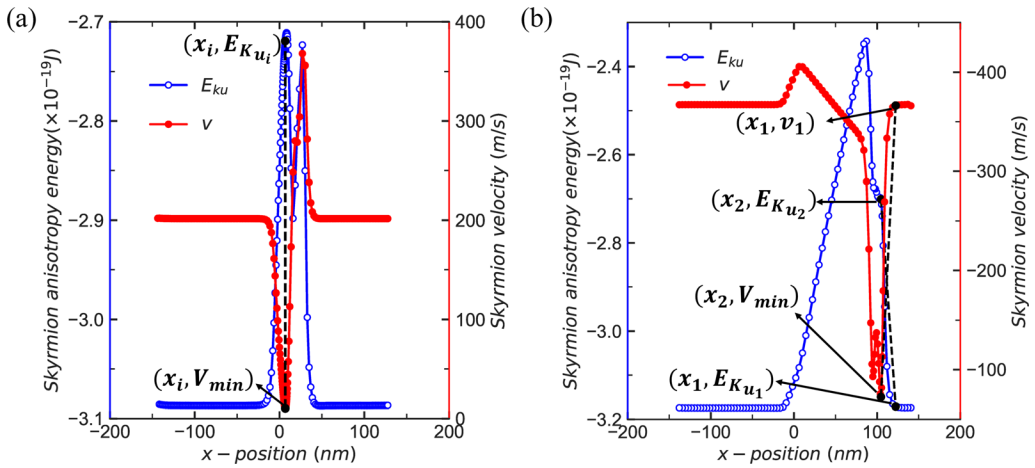

FIG. 4. (a) The PMA energy and the velocity as functions of the position of skyrmion at $J_{spin} = 11\,\mathrm{MA/cm^2}$, $L = 20\,\mathrm{nm}$, and $\Delta K = 0.08\,\mathrm{MJ/m^3}$. (b) The PMA energy and the velocity as functions of the position of skyrmion at $J_{spin} = -20\,\mathrm{MA/cm^2}$, $L = 100\,\mathrm{nm}$, and $\Delta K = 0.08\,\mathrm{MJ/m^3}$.

where the velocity reaches minimum. Meanwhile, the PMA energy increases almost linearly when the skyrmion moves from x_1 to x_2. Therefore, the average force induced by the inhomogeneous PMA energy on skyrmion in the distance $(x_1 - x_2)$ and the minimum velocity of skyrmion during the negative motion are expressed as

$$\overline{F}_{VGF} = \frac{\gamma_0}{4\pi\mu_0 M_s}\frac{\Delta E_{K_u}}{\Delta x}, \tag{8}$$

$$V_{\min} = kJ + \eta,\ J < 0, \tag{9}$$

where $\frac{\Delta E_{Ku}}{\Delta x} = \frac{E_{Ku_1} - E_{Ku_2}}{x_1 - x_2}$, $k = \frac{I_{xy}}{2\alpha D_{xx}}\frac{u(J)}{aJ}$, $\eta = \frac{-1}{\alpha D_{xx}}\overline{F}_{VGF}$, and the relevant parameters are given in Tables SII and SIV in the supplementary material. It is found that the values of $V_{\min}$ calculated by Eq. (9) fit the simulation results well, as illustrated in Fig. 3.

By comparing Figs. 4(b) and 5(a), we find when the skyrmion passes through the same voltage gate positively and negatively, the variations of the PMA energy with the position of skyrmion are very similar. For the blue curve ($L = 100\,\mathrm{nm}$) in Fig. 5(a), the process from P_i to P_m represents the positive entry of skyrmion into the voltage gate, while the process from P_e to P_d represents the negative entry. The absolute values of the slopes of the curve within these two processes denote the average resistance forces on the skyrmion when the skyrmion enters the voltage gate positively and negatively, expressed by F_+ and F_-, respectively. It is found that F_+ increases significantly and F_- decreases slightly as L varies from 100 to 20 nm. Both F_+ and F_- increase with increasing ΔK, as shown in Fig. 5(b). Moreover, F_- is much larger than F_+ when L and ΔK are determined, which is consistent with our previous results.

In conclusion, we have numerically and theoretically investigated the dynamics of current-driven skyrmion passing through a voltage gate in an SAF racetrack. Our results demonstrate that the critical current of skyrmion passing through a voltage gate positively is much

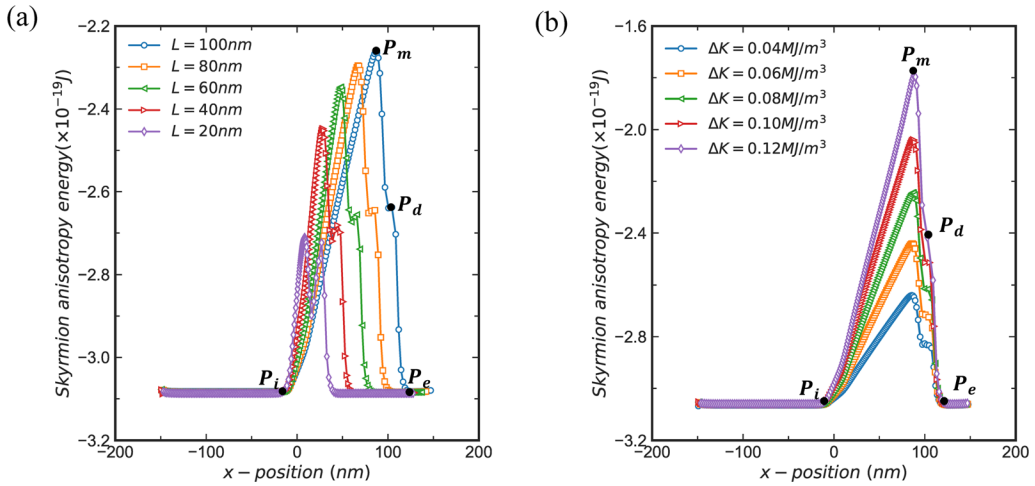

FIG. 5. (a) The PMA energy as a function of the position of skyrmion under various L and $J = 11\,\mathrm{MA/cm^2}$. (b) The PMA energy as a function of the position of skyrmion under various ΔK and $J = 8\,\mathrm{MA/cm^2}$.

smaller than that of skyrmion passing through the gate negatively. In addition, the minimum velocity of skyrmion has linear relationship with the driving current density and the PMA gradient when the skyrmion passes through different voltage gates in both positive and negative directions, and the calculation results are in good agreement with the simulation results. Furthermore, we have found that the driving current density–minimum velocity characteristics of the skyrmion diode are similar to the volt–ampere characteristics of electronic diode. Finally, we have studied the variation of the PMA energy with the position during the positive and negative motion of skyrmion, which helps us to compare the magnitude of resistance force as the skyrmion passes through different voltage gates. These results may play an important role for the design of skyrmion diodes.

See the supplementary material for more results on the anisotropy curve along the racetrack, the velocity as a function of the location of skyrmion, as well as the relevant parameters.

AUTHOR DECLARATIONS

Conflict of Interest

The authors have no conflicts to disclose.

Author Contributions

Min Xu: Formal analysis (equal); Project administration (equal); Supervision (equal); Writing – review & editing (equal). **Zhiyu Zhang:** Conceptualization (equal); Formal analysis (equal); Investigation (equal); Software (equal); Visualization (equal); Writing – original draft (equal). **Jinyu Zhang:** Investigation (equal); Resources (equal). **Guiqian Jiang:** Software (equal); Visualization (equal). **Yuliang Chen:** Resources (equal); Visualization (equal). **Wenlong Chen:** Software (equal); Visualization (equal). **Changjing Hu:** Software (equal); Visualization (equal).

DATA AVAILABILITY

The data that support the findings of this study are available from the corresponding authors upon reasonable request.

REFERENCES

[1]A. Fert, N. Reyren, and V. Cros, Nat. Rev. Mater. **2**, 17031 (2017).
[2]J. Iwasaki, M. Mochizuki, and N. Nagaosa, Nat. Nanotech. **8**, 742 (2013).
[3]N. Nagaosa and Y. Tokura, Nat. Nanotech. **8**, 899 (2013).
[4]W. Koshibae and N. Nagaosa, Nat. Commun. **5**, 5148 (2014).
[5]S. Komineas and N. Papanicolaou, Phys. Rev. B **92**, 064412 (2015).
[6]S. Mühlbauer, B. Binz, F. Jonietz, C. Pfleiderer, A. Rosch, A. Neubauer, R. Georgii, and P. Böni, Science **323**, 915 (2009).
[7]K. Litzius, J. Leliaert, P. Bassirian, D. Rodrigues, S. Kromin, I. Lemesh, J. Zazvorka, K. J. Lee, J. Mulkers, N. Kerber, D. Heinze, N. Keil, R. M. Reeve, M. Weigand, B. V. Waeyenberge, G. Schütz, K. Everschor-Sitte, G. S. D. Beach, and M. Kläui, Nat. Electron. **3**, 30 (2020).
[8]S. Kandukuri, V. S. N. Murthy, and P. K. Thiruvikraman, Sci. Rep. **11**, 18945 (2021).
[9]F. Büttner, C. Moutafis, M. Schneider, B. Krüger, C. M. Günther, J. Geilhufe, C. v. K. Schmising, J. Mohanty, B. Pfau, S. Schaffert, A. Bisig, M. Foerster, T. Schulz, C. A. F. Vaz, J. H. Franken, H. J. M. Swagten, M. Kläui, and S. Eisebitt, Nat. Phys. **11**, 225 (2015).
[10]C. Cheng, Z. Yan, J. Dong, Y. Liu, Z. Xia, L. Li, and X. Han, Phys. Rev. B **104**, 174409 (2021).
[11]S. A. Osorio, M. B. Sturla, H. D. Rosales, and D. C. Cabra, Phys. Rev. B **99**, 064439 (2019).
[12]W. Kang, Y. Huang, C. Zheng, W. Lv, N. Lei, Y. Zhang, X. Zhang, Y. Zhou, and W. Zhao, Sci. Rep. **6**, 23164 (2016).
[13]R. Tomasello, E. Martinez, R. Zivieri, L. Torres, M. Carpentieri, and G. Finocchio, Sci. Rep. **4**, 6784 (2014).
[14]A. Fert, V. Cros, and J. Sampaio, Nat. Nanotech. **8**, 152 (2013).
[15]S. Zhou, C. Zheng, X. Chen, and Y. Liu, J. Appl. Phys. **128**, 033907 (2020).
[16]L. Shen, J. Xia, G. Zhao, X. Zhang, M. Ezawa, O. A. Tretiakov, X. Liu, and Y. Zhou, Appl. Phys. Lett. **114**, 042402 (2019).
[17]S. Zhang, J. Wang, Q. Zheng, Q. Zhu, X. Liu, S. Chen, C. Jin, Q. Liu, C. Jia, and D. Xue, New J. Phys. **17**, 023061 (2015).
[18]D.-H. Jung, H.-S. Han, N. Kim, G. Kim, S. Jeong, S. Lee, M. Kang, M.-Y. Im, and K.-S. Lee, Phys. Rev. B **104**, L060408 (2021).
[19]Y. Feng, X. Zhang, G. Zhao, and G. Xiang, IEEE Trans. Electron Devices **69**, 1293 (2022).
[20]L. Zhao, X. Liang, J. Xia, G. Zhao, and Y. Zhou, Nanoscale **12**, 9507 (2020).
[21]W. Legrand, D. Maccariello, F. Ajejas, S. Collin, A. Vecchiola, K. Bouzehouane, N. Reyren, V. Cros, and A. Fert, Nat. Mater. **19**, 34 (2020).
[22]L. Peng, K. Karube, Y. Taguchi, N. Nagaosa, Y. Tokura, and X. Yu, Nat. Commun. **12**, 6797 (2021).
[23]H. Zhang, D. Raftrey, Y.-T. Chan, Y.-T. Shao, R. Chen, X. Chen, X. Huang, J. T. Reichanadter, K. Dong, S. Susarla, L. Caretta, Z. Chen, J. Yao, P. Fischer, J. B. Neaton, W. Wu, D. A. Muller, R. J. Birgeneau, and R. Ramesh, Sci. Adv. **8**, eabm7103 (2022).
[24]G. Chen, Nat. Phys. **13**, 112 (2017).
[25]W. Jiang, X. Zhang, G. Yu, W. Zhang, X. Wang, M. B. Jungfleisch, J. E. Pearson, X. Cheng, O. Heinonen, K. L. Wang, Y. Zhou, A. Hoffmann, and S. G. E. te Velthuis, Nat. Phys. **13**, 162 (2017).
[26]R. Juge, S.-G. Je, D. de Souza Chaves, L. D. Buda-Prejbeanu, J. Peña-Garcia, J. Nath, I. M. Miron, K. G. Rana, L. Aballe, M. Foerster, F. Genuzio, T. O. Menteş, A. Locatelli, F. Maccherozzi, S. S. Dhesi, M. Belmeguenai, Y. Roussigné, S. Auffret, S. Pizzini, G. Gaudin, J. Vogel, and O. Boulle, Phys. Rev. Appl. **12**, 044007 (2019).
[27]S. Li, J. Xia, X. Zhang, M. Ezawa, W. Kang, X. Liu, Y. Zhou, and W. Zhao, Appl. Phys. Lett. **112**, 142404 (2018).
[28]L. Li, L. Chen, R. Liu, and Y. Du, Chin. Phys. B **29**, 117102 (2020).
[29]X. Zhang, J. Müller, J. Xia, M. Garst, X. Liu, and Y. Zhou, New J. Phys. **19**, 065001 (2017).
[30]C. C. I. Ang, W. Gan, and W. S. Lew, New J. Phys. **21**, 043006 (2019).
[31]X. Wang, W. L. Gan, J. C. Martinez, F. N. Tan, M. B. A. Jalil, and W. S. Lew, Nanoscale **10**, 733 (2018).
[32]J. Wang, J. Xia, X. Zhang, X. Zheng, G. Li, L. Chen, Y. Zhou, J. Wu, H. Yin, R. Chantrell, and Y. Xu, Appl. Phys. Lett. **117**, 202401 (2020).
[33]A. G. Kolesnikov, M. E. Stebliy, A. S. Samardak, and A. V. Ognev, Sci. Rep. **8**, 16966 (2018).
[34]K. Litzius, I. Lemesh, B. Krüger, P. Bassirian, L. Caretta, K. Richter, F. Büttner, K. Sato, O. A. Tretiakov, J. Förster, R. M. Reeve, M. Weigand, I. Bykova, H. Stoll, G. Schütz, G. S. D. Beach, and M. Kläui, Nat. Phys. **13**, 170 (2017).
[35]M. Shen, Y. Zhang, J. Ou-Yang, X. Yang, and L. You, Appl. Phys. Lett. **112**, 062403 (2018).
[36]X. Zhang, J. Xia, Y. Zhou, D. Wang, X. Liu, W. Zhao, and M. Ezawa, Phys. Rev. B **94**, 094420 (2016).
[37]J. Xia, X. Zhang, M. Ezawa, Z. Hou, W. Wang, X. Liu, and Y. Zhou, Phys. Rev. Appl. **11**, 044046 (2019).
[38]W. Koshibae and N. Nagaosa, Sci. Rep. **7**, 42645 (2017).
[39]C. Jin, C. Song, J. Wang, and Q. Liu, Appl. Phys. Lett. **109**, 182404 (2016).
[40]L. Shen, X. Li, Y. Zhao, J. Xia, G. Zhao, and Y. Zhou, Phys. Rev. Appl. **12**, 064033 (2019).
[41]R. Cacilhas, V. L. Carvalho-Santos, S. Vojkovic, E. B. Carvalho, A. R. Pereira, D. Altbir, and Á. S. Núñez, Appl. Phys. Lett. **113**, 212406 (2018).
[42]F. Ando, M. Ishibashi, T. Koyama, Y. Shiota, T. Moriyama, D. Chiba, and T. Ono, Appl. Phys. Lett. **113**, 252402 (2018).
[43]D. Chiba, M. Kawaguchi, S. Fukami, N. Ishiwata, K. Shimamura, K. Kobayashi, and T. Ono, Nat. Commun. **3**, 888 (2012).
[44]K. Yamada, S. Murayama, and Y. Nakatani, Appl. Phys. Lett. **108**, 202405 (2016).
[45]M. Weisheit, S. Fähler, A. Marty, Y. Souche, C. Poinsignon, and D. Givord, Science **315**, 349 (2007).

[46]T. Hirai, T. Koyama, A. Obinata, Y. Hibino, K. Miwa, S. Ono, M. Kohda, and D. Chiba, Appl. Phys. Express **9**, 063007 (2016).
[47]T. Maruyama, Y. Shiota, T. Nozaki, K. Ohta, N. Toda, M. Mizuguchi, A. A. Tulapurkar, T. Shinjo, M. Shiraishi, S. Mizukami, Y. Ando, and Y. Suzuki, Nat. Nanotech. **4**, 158 (2009).
[48]J. H. Guo, J. Xia, X. Zhang, P. W. T. Pong, and Y. Zhou, Phys. Lett. A **392**, 127157 (2021).
[49]D. Das, B. Muralidharan, and A. Tulapurkar, J. Magn. Magn. Mater. **491**, 165608 (2019).
[50]C. Song, C. Jin, J. Wang, Y. Ma, H. Xia, J. Wang, J. Wang, and Q. Liu, Appl. Phys. Express **12**, 083003 (2019).
[51]M. Beg, M. Lang, and H. Fangohr, IEEE Trans. Magn. **58**, 1 (2022).
[52]H. Xia, C. Song, C. Jin, J. Wang, J. Wang, and Q. Liu, J. Magn. Magn. Mater. **458**, 57 (2018).